THE JOURNAL OF PHYSICAL CHEMISTRY A

Article

pubs.acs.org/JPCA

Ultrafast Excited-State Dynamics of Donor–Acceptor Biaryls: Comparison between Pyridinium and Pyrylium Phenolates

Romain Letrun,[†] Marius Koch,[†] Marina L. Dekhtyar,[‡] Vladimir V. Kurdyukov,[‡] Alexei I. Tolmachev,[‡] Wolfgang Rettig,[§,*] and Eric Vauthey[†,*]

[†]Department of Physical Chemistry, University of Geneva, 30 quai Ernest-Ansermet, CH-1211 Geneva 4, Switzerland

[‡]Institute of Organic Chemistry, National Academy of Sciences of Ukraine, Murmanskaya str. 5, Kiev, 02094, Ukraine

[§]Institut für Chemie der Humboldt-Universität Berlin, Brook-Taylor-Strasse 2, D-12489 Berlin, Germany

Supporting Information

ABSTRACT: The excited-state dynamics of two donor–acceptor biaryls that differ by the strength of the acceptor, a pyridinium or a pyrylium moiety, have been investigated using a combination of steady-state solvatochromic absorption, ultrafast fluorescence, as well as visible and infrared transient absorption spectroscopies. The negative solvatochromic behavior of pyridinium phenolate indicates that the permanent electric dipole moment experiences a decrease upon $S_1 \leftarrow S_0$ excitation, implying that the ground state possesses more zwitterionic character than the excited state. In contrast, pyrylium phenolate exhibits a weakly positive solvatochromic behavior corresponding to a small increase in the dipole moment upon excitation, implying more zwitterionic character in the excited than the ground state. Both compounds are therefore situated at different sides of the cyanine-limit structure, which has equally polar ground and excited states. Despite these differences, both molecules exhibit qualitatively similar excited-state properties. They are characterized by a very short fluorescence lifetime, increasing from about 1 to 20 ps, when varying solvent viscosity from 0.4 to 11 cP. There are, however, characteristic differences between the two compounds: The excited-state lifetimes of the pyrylium dye are shorter and also depend somewhat on polarity. The ensemble of spectroscopic data can be explained with a model where the emitting Franck–Condon excited state relaxes upon twisting around the single bond between the aryl units to a point where the excited- and ground-state surfaces are very close or intersect. After internal conversion to the ground state, the distorted molecule relaxes back to its equilibrium planar configuration, again largely dependent upon solvent viscosity. However, in this case, the kinetics for the pyrylium dye are slower than for the pyridinium dye and the polar solvent-induced acceleration is significantly stronger than in the excited state. This difference of kinetic behavior between the two compounds is a direct consequence of the change of the electronic structure from a *normal* to an *overcritical* merocyanine evidenced by steady-state spectroscopy.

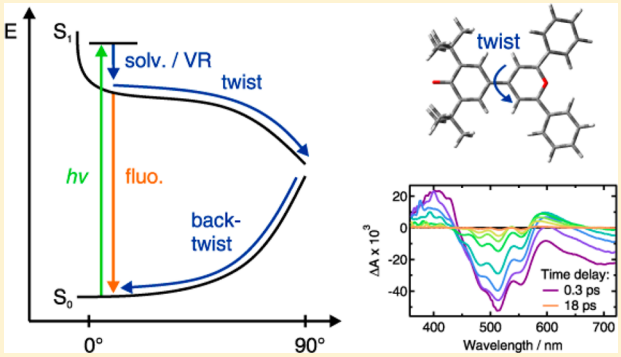

INTRODUCTION

Donor–acceptor biaryls are push–pull molecules that, because of their large hyperpolarizability, offer promising perspectives for the development of nonlinear optical materials.[1−6] For such applications, a deep understanding of the structure-properties relationship is required. Betaine-30, also known as Reichardt's dye, is the most famous example of this family. Its renown comes from the huge solvent dependence of its $S_1 \leftarrow S_0$ transition energy, which is being used as the $E_T(30)$ empirical polarity scale.[7] This very large solvatochromism arises from the zwitterionic character of its ground state and from the small electric dipole moment of its S_1 state, resulting in a strong charge-transfer character of this transition, the phenolate and pyridinium units acting as electron donor and acceptor, respectively. The lack of fluorescence of betaine-30 has attracted the attention of several groups, which have investigated its excited-state dynamics by ultrafast optical spectroscopy and quantum chemistry calculations.[8−15] For example, Barbara and co-workers have rationalized the transient absorption dynamics measured at a single wavelength with a model where the nonradiative deactivation of the excited state is a charge separation process whose dynamics is entangled with that of solvent relaxation.[8−10] The slowing down of the dynamics observed by decreasing temperature and going from ethanol to longer alcohols was explained in terms of longer solvent relaxation times. Subsequent investigations by Ernsting and co-workers using broadband transient absorption revealed complex dynamics that could not be fully captured by previous single wavelength experiments and evidenced the importance of structural rearrangements.[12] Indeed, the excited-state dynamics

Received: September 27, 2013
Revised: November 16, 2013
Published: November 19, 2013

   dx.doi.org/10.1021/jp409646g | J. Phys. Chem. A 2013, 117, 13112−13126

Scheme 1. Structure of the Pyridinium Phenolate (1), Its Desphenyl Analogue (1a), and Pyrylium Phenolate (2)[a]

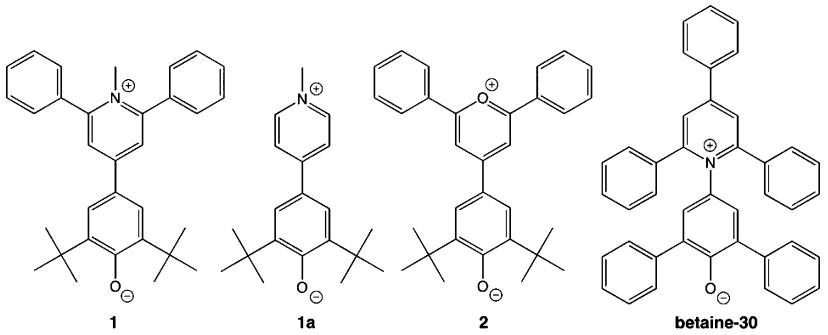

[a]The structure of betaine-30 is also given for comparison.

of betaine-30 involves conformational changes during its evolution from the Franck−Condon excited state populated upon photoexcitation to a twisted relaxed excited state, characterized by a close to 90° dihedral angle between the donor and acceptor rings, that decays to the unrelaxed ground state, itself reverting to the original planar conformation. A similar behavior has been observed with various zwitterionic pyridinium phenolates and with their cationic phenol counterparts.[16,17] It has been shown that it is possible to modulate the excited-state dynamics of these molecules by using steric hindrance to introduce a twist in their ground-state structure.[16,17] Increasing the pretwist leads to a shortening of the excited-state lifetime as the Franck−Condon excited-state structure is getting more similar to that of the twisted relaxed excited state.

In this contribution, we report on our investigation of the excited-state dynamics of two newly synthesized donor−acceptor biaryl systems that are characterized by bulky substituents and by a difference in their acceptor strength (Scheme 1) using a combination of steady-state and femtosecond time-resolved spectroscopic techniques covering the visible and infrared domains, and quantum chemical calculations. The main aim of this study was to investigate the effect of the donor−acceptor strength that increases when going from pyridinium (**1**) to pyrylium phenolate (**2**) on the excited-state dynamics of donor−acceptor biaryl systems. We will show that their different donor−acceptor strength leads to substantial dissimilarities in the nature of both the ground and excited states. As a result, the excited-state dynamics of the structural changes, though dominated by similar steric parameters, quantitatively differs for the two compounds.

EXPERIMENTAL SECTION

Synthesis of the dyes. *2,6-Di-tert-butyl-4-(1-methyl-2,6-diphenylpyridinium-4-yl)benzenolate (**1**).* To a solution of 0.322 g (0.6 mmol) of 4-(3,5-di-*tert*-butyl-4-hydroxyphenyl)-2,6-diphenylpyrylium perchlorate[18] in 2 mL of acetonitrile, 1.5 mL of a methanol solution of methylamine was added. After heating at 80 °C for 1 h and cooling, the salt was precipitated by a saturated aqueous solution of sodium perchlorate, filtered, washed with water, and dissolved in acetonitrile. Then 1 mL of triethylamine was added, and the mixture was stirred for 10 min and poured into 120 mL of water. After 12 h, the precipitate was filtered, washed with water, and dried. The product was purified by column chromatography on alumina from chloroform. Crystallized from acetonitrile. Yield: 0.124 g (46%). Mp: 259−262 °C. λ_{max} ($\varepsilon \times 10^{-4}$ M^{-1} cm^{-1}) in CH_3CN: 274(1.41); 517(5.72). ^1H NMR in $CDCl_3$, δ, ppm: 1.389 (s, 18H, *t*-Bu); 3.187 (s, 3H, NMe); 7.070 (s, 2H, β-H); 7.437 (s, 2H, β'-H); 7.453−7.500 (m, 4H, Ar−H); 7.551−7.572 (m, 6H, Ar−H). Anal. Found: C, 85.26; H, 7.75; N, 3.19. Calcd for $C_{32}H_{35}NO$: C, 85.48; H, 7.85; N, 3.12. $m/z = [M + 1]^+ = 450.3$; $m/z = [M + 2]^+ = 451.2$; calculated for $C_{32}H_{35}NO$, 449.27; found, 449.3.

*2,6-Di-tert-butyl-4-(2,6-diphenylpyrylium-4-yl)-benzenolate (**2**).* To a solution of 0.322 g (0.6 mmol) of 4-(3,5-di-*tert*-butyl-4-hydroxyphenyl)-2,6-diphenylpyrylium perchlorate[18] in 6 mL of acetonitrile, 1 mL of triethylamine was added. The reaction mixture was stirred for 10 min and poured into 120 mL of water. After 12 h, the precipitate was filtered, washed with water, and dried. The dye was purified by column chromatography on alumina from chloroform. Crystallized from acetonitrile. Yield: 0.194 g (74%). Mp: 248−250 °C. λ_{max} ($\varepsilon \times 10^{-4}$ M^{-1} cm^{-1}) in CH_3CN: 323 (1.83); 482 (3.72); 510 (4.04); 550 (2.48, shoulder). ^1H NMR in acetone-d_6, δ, ppm: 1.319 (s, 18H, *t*-Bu); 7.508−7.542 (m, 6H, Ar−H); 7.589 (s, 2H, β-H); 7.667 (s, 2H, β'-H); 8.010−8.042 (m, 4H, Ar−H). Anal. Found C, 85.07; H, 7.29. Calcd for $C_{31}H_{32}O_2$: C, 85.26; H, 7.39. $m/z = [M + 1]^+ = 437.3$; calculated for $C_{31}H_{32}O_2$, 436.27; found, 436.3.

Solvents. The solvents, acetonitrile (ACN, Roth, ≥99.9%), ethanol (EtOH, Fluka, ≥99.8%), 1-pentanol (PeOH, Sigma-Aldrich, ≥99%), 1-octanol (OcOH, Fluka, ≥99.5%), 1-decanol (DeOH, Alfa Aesar, ≥98%), tetrahydrofuran (THF, Sigma-Aldrich, ≥99.9%), chloroform ($CHCl_3$, Sigma-Aldrich, ≥99%), diethyl ether (Et_2O, Sigma-Aldrich, ≥99.8%), dibutyl ether (Bu_2O, Acros Organics, ≥99%), cyclohexane (CHX, Acros Organics, ≥99.5%) and dodecane (DD, Acros Organics, ≥99%) were used as received.

Steady-State Spectroscopy. Electronic absorption spectra were recorded on a Cary 50 spectrophotometer.

Fluorescence Up-Conversion (FU). The up-conversion setup has been described in detail previously.[16,19] Excitation was performed at 500 nm using the frequency doubled output of a Kerr lens mode locked Ti:sapphire laser (Mai Tai HP, Spectra Physics). The polarization of the pump pulses was at magic angle relative to that of the probe pulses at 1000 nm. The pump intensity on the sample was about 5 μJ cm^{-2} and the full width at half-maximum (fwhm) of the instrument response function was ca. 230 fs. The samples were placed in a 0.4 mm rotating cell and had an absorbance between 0.2 and 0.5 at the excitation wavelength. No sample degradation was observed throughout the measurements.

Visible Transient Absorption (TA). The femtosecond visible TA setup has been described in detail previously.[20,21]

Excitation was carried out at 500 or 520 nm with a home-built two-stage noncollinear optical parametric amplifier. The pump intensity on the sample was about 1 mJ cm^{-2}. The polarization of the pump pulses was at magic angle relative to that of the probe pulses. All spectra were corrected for the group velocity dispersion of the white light continuum. The fwhm of the response function was ca. 200 fs. The samples were located in a 1 mm quartz cell, continuously stirred by nitrogen bubbling, and their absorbance was between 0.2 and 0.5 at the excitation wavelength. No significant degradation of the samples was observed throughout the measurements.

Infrared Transient Absorption (IR TA). The femtosecond visible pump/mid-IR probe transient absorption setup is based on an amplified Ti:sapphire system (800 nm, 1 kHz repetition rate and 100 fs pulse width, Solstice, Spectra Physics). Part of this output was frequency doubled to provide pump pulses at 400 nm with an energy between 2 and 4 μJ. The pulses were focused to a 300 μm diameter spot on the sample. Another part of the amplifier output was used to pump an optical parametric amplifier (TOPAS-C, Light Conversion), whose output was difference-frequency mixed (NDFG module, Light Conversion) to generate mid-IR probe pulses centered at 6.21 μm with a width of 400 nm. The horizontally polarized mid-IR pulses were split into two and focused to a 140 μm diameter spot on the sample. One of the mid-IR beams was overlapped with the pump beam at magic angle, whereas the second one was used as reference beam. Both probe beams were dispersed with a spectrograph (Triax 190, 150 lines/mm, Horiba) equipped with a liquid nitrogen cooled 2 × 64 element MCT array (Infrared Systems Development) giving a resolution of 1−2 cm^{-1}. The sample area and the detection system were located in a box that was purged with dry air for at least 45 min before each experiment. Throughout the measurements, every second pump pulse was blocked and the average of 5000 signal shots was taken to collect one data point. At least 15 measurements for each system were averaged to reconstruct the spectra. To provide a new sample solution for each shot, a flow cell as described in ref 22 was used. The absorbance at the excitation wavelength was below 0.15 on 200 μm, the sample cell thickness.

Quantum Chemistry Calculations. Ground-state gas-phase geometry optimization was performed at the density functional level of theory (DFT) using the CAM-B3LYP functional and the cc-pVDZ basis set. Electronic vertical excitation energies were computed with time-dependent density functional theory (TD-DFT) using the same functional and basis set. The calculations were carried out using the Gaussian 09 package.[23]

RESULTS

Steady-State Spectroscopy. The stationary electronic absorption spectra of **1** and **2** in solvents of varying polarity are shown in Figure 1. The absorption spectrum of **1** in the visible region consists of a single broad band with a maximum between 510 and 535 nm. The shape of this band that can be ascribed to the $S_1 \leftarrow S_0$ transition exhibits a significant solvent dependence: it is broad and structureless in CHX and becomes structured with a ∼1300 cm^{-1} vibrational progression in low polarity solvents, such as Et_2O and $CHCl_3$. The relative intensity of the 0−0 vibronic band decreases considerably when increasing solvent polarity further. In polar solvents, *i.e.*, EtOH and ACN, the vibronic structure is no longer visible and the band is about twice as narrow as in CHX. The apparent solvatochromic

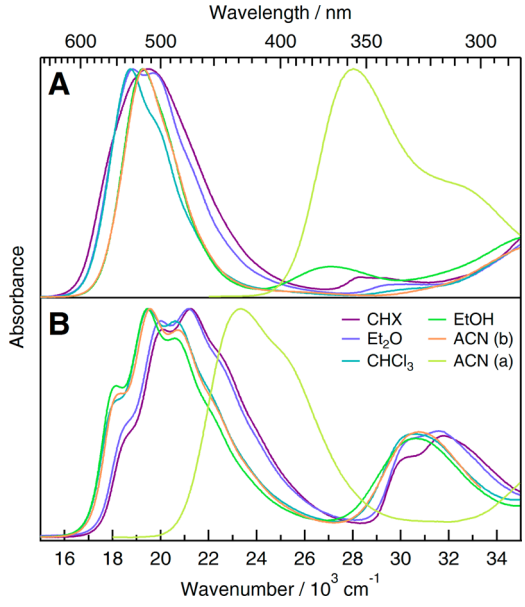

Figure 1. Absorption spectra of **1** (A) and **2** (B) in various solvents. The labels (b) and (a) refer to basic and acidic forms, respectively.

behavior of the absorption maximum for **1** is complicated, first positive and then negative, corresponding first to a red shift upon increasing the dielectric constant of the solvent, and then to a blue shift when going to the most polar solvents (Table 1).

Table 1. Solvent Dielectric Constant (ε_s)[a], Viscosity (η/cP)[a], Absorption Maximum ($\bar{\nu}_{max}/10^3$ cm^{-1}), and 0−0 Absorption Maximum ($\bar{\nu}_{00}/10^3$ cm^{-1}) Obtained from Bandshape Analysis

			1		2	
solvent	ε_s	η	$\bar{\nu}_{max}$	$\bar{\nu}_{00}$	$\bar{\nu}_{max}$	$\bar{\nu}_{00}$
dodecane (DD)	2.01	1.38	19.5	18.1	21.2	18.4
cyclohexane (CHX)	2.02	0.89	19.6	18.2	21.2	18.5
dibutyl ether (Bu_2O)	3.08	0.64	19.5	18.2	21.1	18.4
diethyl ether (Et_2O)	4.27	0.22	18.8	18.8	20.0	18.6
chloroform ($CHCl_3$)	4.81	0.54	18.7	18.7	19.5	18.1
tetrahydrofuran (THF)	7.52	0.46	18.8	18.8	19.6	18.3
decanol (DeOH)	7.93	10.9	18.8	18.8	19.4	18.0
octanol (OcOH)	10.30	7.3	18.9	18.9	19.7	18.4
pentanol (PeOH)	15.13	3.6	19.0	19.0	19.4	18.0
ethanol (EtOH)	25.30	1.08	19.3	19.3	19.4	18.1
acetonitrile (ACN, basic)	36.64	0.37	19.3	19.3	19.5	18.2
acetonitrile (acidic)	36.64	0.37	28.0	28.0	23.2	21.9

[a]From ref 26.

Relying on band maxima only is dangerous and can lead to incorrect conclusions if the spectral shape changes with solvent polarity. This problem can be avoided by using instead the 0−0 transition energy, $\bar{\nu}_{00}$. To determine $\bar{\nu}_{00}$ and its solvent dependence, the band shape was analyzed using a sum of Gaussian functions. A plot of the so-obtained 0−0 transition energy vs. $[f(\varepsilon_s) - f(n^2)]$, where $f(x) = (x - 1)/(x + 2)$ and ε_s and n are the static dielectric constant and the refractive index, respectively, exhibits a reasonably linear dependence with a slope of 1605 ± 165 cm^{-1} for compound **1**, indicating a moderately negative solvatochromic behavior, *i.e.* a blue shift upon increasing solvent polarity, in the whole range of solvent

dx.doi.org/10.1021/jp409646g | J. Phys. Chem. A 2013, 117, 13112−13126

polarities (Figure S1, Supporting Information). Such a behavior is indicative of a reduction of the dipole moment upon photoexcitation and is typical for molecules with a predominantly zwitterionic ground state.[7,24]

The negative solvatochromism of **1** is much weaker than that of betaine-30, for which the slope of the transition energy vs $[f(\varepsilon_s)\text{-}f(n^2)]$, determined with the same solvents, amounts to 10060 ± 1700 cm^{-1}. It is also substantially smaller than for **1a**, the analogue of **1** without the two phenyl substituents, for which a solvatochromic slope of 2400 cm^{-1} has been reported.[25]

The absorption spectrum of **1** in EtOH and other protic solvents exhibits a second, less intense, band at ∼370 nm, which is assigned to the protonated form, **H-1**, of **1**. Indeed, addition of NaOH to the solution (100 μL 1 M NaOH in 3 mL) leads to the suppression of this band. On the other hand, addition of HCl to an ACN solution of **1** (100 μL 1 M HCl in 3 mL) results in a totally new absorption spectrum with a broad band culminating around 360 nm. Protonation of the phenolate moiety diminishes its electron-donating ability and consequently leads to a blue shift of the absorption transition as outlined in detail in the discussion section.

Only very weak stationary fluorescence with a quantum yield below 10^{-4} was measured for **1**. The fluorescence band is very broad and unstructured and extends from ∼570 to 800 nm in CHX (Figure S2). As will be shown below, this very small fluorescence quantum yield is due to the ultrafast decay of the emitting population. The solvatochromism of the fluorescence was not investigated because a large fraction of the emission occurs from the nonrelaxed excited state (see below).

The absorption spectrum of **2** consists of two bands, with the most intense one around 500 nm assigned to the $S_1 \leftarrow S_0$ transition and a further band around 320 nm. Contrary to **1**, the vibrational progression can be easily observed in all solvents. This makes it easy to see that the relative intensity of the vibronic bands depends on the solvent, with the 0−0 band rising in relative intensity for an increase of polarity. The $S_1 \leftarrow S_0$ band maximum coincides with the second vibronic transition (1−0 band) in polar solvents and with the third one in the less polar solvents. This suggests substantial variation of the Franck−Condon factor with solvent polarity that could be indicative of a solvent dependence of the ground-state structure like, *e.g.*, a more quinoid structure in nonpolar and low to medium polarity solvents and an equalized-bond structure in solvents of high polarity. Bandshape analysis using a sum of Gaussian functions reveals that the $S_1 \leftarrow S_0$ 0−0 transition energy, $\bar{\nu}_{00}$, decreases only weakly with increasing the dielectric constant of the solvent (weak positive solvatochromism). The plot of $\bar{\nu}_{00}$vs $[f(\varepsilon_s)\text{-}f(n^2)]$ shows a substantial scattering and a linear fit yields a slope of −539 ± 216 cm^{-1} (Figure S1, Supporting Information). Therefore, compounds **1** and **2** exhibit an opposite solvatochromism. Whereas the ground state of **1** is predominantly zwitterionic, that of **2** is rather non polar. These aspects will be discussed in more detail below using the *cyanine limit model*.[27]

The absorption band of the protonated form of **2**, **H-2**, peaks at 430 nm, *i.e.*, is closer to the band of the phenolate form than in the case of **1**. This smaller energy difference between the acidic and basic forms of **2** is in agreement with the stronger acceptor character of the pyrylium moiety, as will be outlined below. Like for **1**, only very weak emission was found with **2** (Figure S3), indicative of the existence of very efficient nonradiative deactivation pathways of the excited state.

Time-Resolved Fluorescence. Figure 2 shows fluorescence time profiles recorded at various wavelengths with **1** in

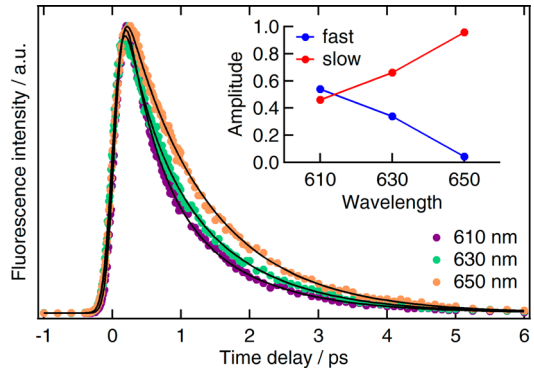

Figure 2. Fluorescence time profiles measured with **1** in ACN at several wavelengths and best multiexponential global fits (solid lines). Inset: wavelength dependence of the amplitudes associated with the fast (0.43 ps) and with the slow (1.2 ps) components.

ACN. These profiles could be analyzed globally using the sum of two exponential functions with 0.43 and 1.2 ps time constants and with the amplitudes illustrated in the inset of Figure 2. The amplitude of the short component decreases strongly with increasing wavelength and almost vanishes at 650 nm, suggesting a dynamic red shift of the emission band. No reliable time profile above 650 nm, where a 0.43 ps rising component could be anticipated, could be recorded because of the weakness of the signal. Such a rise time combined with a fast decay time, *i.e.*, 1.2 ps, could explain the weakness of the FU signal. As a consequence, the short time constant is assigned to a dynamic Stokes shift due to solvent relaxation, whereas the longer time constant is ascribed to the decay of the population of the emitting state. This interpretation is supported by the charge-transfer character of the transition and by the similarity of the 0.43 ps time constant with that of 0.63 ps reported for the diffusive solvation time of ACN.[28] A qualitatively similar behavior was measured with **2** in ACN with a 0.39 ps component decreasing in relative amplitude with increasing wavelength, ascribed to solvent relaxation as well, and a 0.83 ps component, assigned to population decay. Given that excitation was performed above the 0−0 transition, vibrational relaxation most probably also contributes to the observed fluorescence time profiles.[29] However, its dynamics does not differ enough from those of solvation and population relaxation to be properly disentangled.

Similar measurements with both **1** and **2** were performed in other solvents of varying polarity and viscosity (Figure 3). For each solvent, the time profiles recorded at 3 to 5 different wavelengths were analyzed globally and could be well reproduced using the sum of two or three exponential functions, with the time constants listed in Table 2. In nonpolar solvents, the fluorescence dynamics of both **1** and **2** exhibited a subpicosecond component with an amplitude decreasing with increasing wavelength. As nonpolar solvation is known to cause minor spectral dynamics, this short component is ascribed to vibrational relaxation. A dynamic Stokes shift was observed with **1** and **2** in all polar solvents. In the long alcohols, PeOH to DeOH, this process was found to be biphasic with **1**, with time constants in good agreement with the solvation times reported in the literature.[28] Because of the shorter excited-state

dx.doi.org/10.1021/jp409646g | J. Phys. Chem. A 2013, 117, 13112−13126

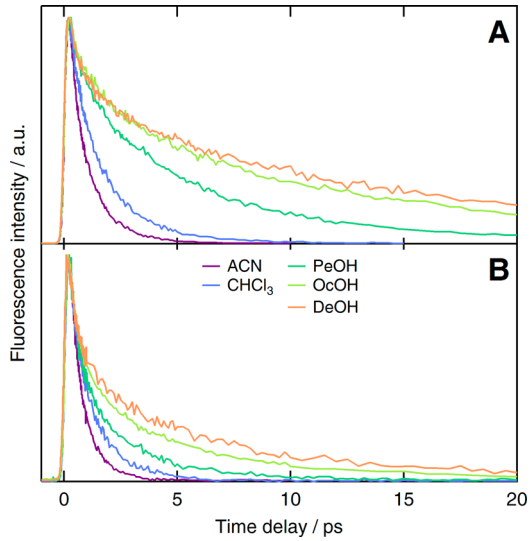

Figure 3. Early fluorescence time profiles measured at 610 nm with (A) **1** and (B) **2** in various solvents.

Table 2. Solvents Dielectric Constant (ε_s)[a], Viscosity (η/cP)[a], Time Constants (τ_i/ps) Obtained from the Global Analysis of the Fluorescence Dynamics of 1 and 2[b]

			1			2	
Solvent	ε_s	η	τ_1	τ_2	τ_3	τ_1	τ_2
dodecane	2.01	1.38	5.4		0.71	3.0	0.32
cyclohexane	2.02	0.89	2.9		0.66	2.3	0.33
chloroform	4.81	0.54	2.0		0.73	1.4	0.47
decanol	7.93	10.9	26	7.6	0.69	6.7	0.57
octanol	10.30	7.3	19	5.7	0.78	5.1	0.53
pentanol	15.13	3.6	9.2	3.7	0.55	2.7	0.53
ethanol	25.30	1.08	2.4		0.85	1.3	0.44
acetonitrile	36.64	0.37	1.2		0.43	0.83	0.39

[a]From ref 26. [b]The longest time constant, τ_1, is assigned to the excited-state lifetime.

lifetime of **2**, only the faster solvation component was observed with this molecule.

From Table 2, it appears that τ_1, the excited-state lifetime of **1** and **2**, increases substantially with the viscosity of the solvent, η, pointing to the involvement of an intramolecular mode with large amplitude motion in the nonradiative deactivation of the emitting state. When the excited-state dynamics is dominated by such a process, the excited-state lifetime usually exhibits a power law dependence with respect to the viscosity:

$$\tau \propto \eta^{\alpha} \quad (1)$$

with $\alpha \leq 1$,[30] $\alpha = 1$ corresponding to the high friction limit of Kramers theory.[31] On the other hand, a α value smaller than unity indicates that the friction exerted by the environment on the molecule is not well described by viscosity and/or that more than one coordinate is involved in the nonradiative deactivation. A systematic decrease of solvent polarity with increasing viscosity, together with a polarity-dependent activation barrier for torsion, have also been shown to lead to a departure from $\alpha = 1$.[32] Figure S4 shows that a plot of $\ln(\tau_1)$ measured with **1** vs $\ln(\eta)$ in all solvents is linear with a slope of $\alpha = 0.90 \pm 0.05$ and a squared correlation coefficient $R^2 = 0.989$. The same plot for **2** yields a smaller slope, $\alpha = 0.53 \pm 0.09$, but does not exhibit such a good linear correlation, $R^2 = 0.928$. The correlation improves substantially, $R^2 = 0.977$, if only the polar solvents are considered, but the slope does not change significantly. This indicates that the fluorescence lifetime of **1** depends mostly on the viscosity of the solvent, whereas that of **2** is additionally affected by solvent polarity. At similar viscosity, the fluorescence lifetime of **2** is about two times longer in nonpolar than in polar solvents.

By comparison, the fluorescence lifetime of **1a**, the analogue of **1** without the two phenyl substituents, exhibits a viscosity dependence with $\alpha = 0.5$ in polar solvents.[16] Figure 3 and Table 2 also reveal that in all solvents investigated, the excited-state lifetime of **2** is systematically smaller than that of **1** by a factor varying from 1.4 to 3.9 depending on the solvent viscosity. Comparatively, the excited-state lifetime of **1a** is shorter than that of **1** by a factor of more than 10.[16]

Visible transient absorption. Figure 4 shows visible TA spectra measured with **1** in ACN at different time delays after excitation at 520 nm. These spectra are dominated by an intense negative band in the 430−570 nm region that can be ascribed to the bleach of the $S_1 \leftarrow S_0$ absorption. At early time (Figure 4A), this negative band exhibits a shoulder at ∼600 nm, which decreases to zero and shifts to ∼650 nm within approximately 1 ps. This band can be assigned to the $S_1 \rightarrow S_0$ stimulated emission. Both its red shift and short lifetime agree with the time-resolved fluorescence measurements. Two positive TA bands can also be observed: one centered around 385 nm, already present at early time and decaying entirely to zero within 7 ps (Figure 4B), and another increasing with the decay of the stimulated emission, peaking initially around 575 nm, and showing first a rapid shift to ∼560 nm with a partial decay (Figure 4B) and then a slower shift to ∼540 nm with a decrease down to zero (Figure 4C). A target analysis of the time evolution of the TA intensity was performed assuming a series of consecutive exponential steps.[33] A good fit could in most cases be achieved assuming three successive steps, *i.e.*, A → B → C → D, with the species- (state-) associated difference spectra (SADS) and time constants shown in Figure 4D and Table 3. The species A decays in 1.3 ps and its spectrum exhibits the 385 nm band, the bleach as well as the stimulated emission band. This species can be identified as the emitting state populated by optical excitation. Its decay time agrees well with that of 1.2 ps obtained from the FU measurements. The 0.43 ps component observed by FU and interpreted as solvent relaxation cannot be observed here. Most probably, the effect of this process on the TA spectra is not marked enough to appear as a significant step in the target analysis.

The spectrum associated with species B, populated from the emitting state, also shows the 385 nm band and the bleach. However, the stimulated emission band is replaced by a positive band peaking at ∼590 nm. Interestingly, the lifetime of B is the same as that of the emitting state. This suggests that the processes responsible for the decay of these two species are of similar nature. The presence of the 385 nm band and of the bleach indicates that B is not largely different from A. As a consequence, this species B is interpreted as a dark excited state. The 385 nm band is absent from the difference absorption spectrum of species C. The latter only exhibits the bleach with a reduced intensity compared to A and B, and a positive band with a maximum at 555 nm. This species decays with a time constant of 3 ps to species D, whose difference absorption spectrum is zero in the entire spectral window. Therefore, D is the ground state, whereas C can be assigned to the unrelaxed ground state. An unrelaxed, or vibrationally hot,

dx.doi.org/10.1021/jp409646g | J. Phys. Chem. A 2013, 117, 13112−13126

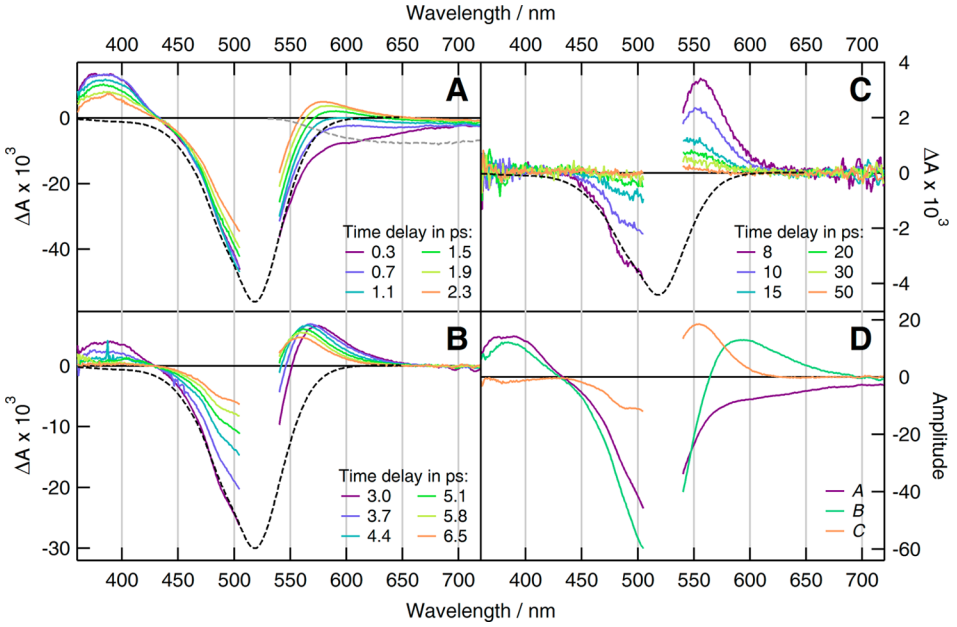

Figure 4. (A–C) Visible TA spectra measured with **1** in ACN and (D) species-associated difference absorption spectra obtained from target analysis. The dashed black line and the dashed gray line represent the scaled stationary absorption and stimulated emission spectra (calculated by multiplying the stationary fluorescence intensity by λ^4),[34] respectively.

Table 3. Time Constants (τ_{XY}/ps) Obtained from the Target Analysis of the Visible and IR TA Spectra Measured with 1 and 2 Assuming 3 or 4 Successive Exponential Steps[b]

	1				2			
solvent	τ_{AB}	τ_{BC}	τ_{CD}	τ_{DE}	τ_{AB}	τ_{BC}	τ_{CD}	τ_{DE}
dodecane	0.85	**2.6**	*13*		0.59	**2.5**	*~42*	
cyclohexane	0.96	**1.6**	*5.4*		0.58	**1.9**	6.8	*~27*
decanol	1.9	**15**	*48*		0.43	**3.1**	*14*	109[a]
pentanol	2.5	**6.3**	*21*		0.56	**2.1**	*8.6*	19[a]
ethanol	**1.0**	3.5	*6.2*		**0.92**	0.92	*7.1*	
acetonitrile	**1.3**	1.3	*3.0*	41[a]	**0.72**	0.72	*4.3*	21[a]

[a]Present in the IR TA data only. [b]The time constants obtained from visible TA data were kept fixed for the analysis of the IR TA data. The interpretation of the time constants is also indicated: **bold**, emissive excited-state lifetime; *italic*, time constant of ground-state relaxation by back-twist; plain, solvent/vibrational relaxation time or dark excited-state lifetime.

ground state is characterized by a positive band located on the red edge of the bleach,[35,36] and is generally observed when the nonradiative deactivation of an excited to the ground state occurs on a faster or similar time scale than that of relaxation.

The TA spectra recorded with **1** in other solvents are qualitatively similar to those in ACN, the main difference being the time scale of the spectral evolution. In all solvents investigated, these TA spectra could also be analyzed using a sequential reaction scheme, with the time constants listed in Table 3. In EtOH, the SADS are mostly the same as in ACN and thus the A–D species can be interpreted alike. In the longer alcohols, *i.e.*, PeOH and DeOH, the spectra of A and B contain the stimulated emission band, that of A being blue-shifted relative to that of B. Moreover, no species without the stimulated emission band but with the 385 nm band could be observed. Therefore, in these two solvents, A is interpreted as the emitting state prior to solvent relaxation, B as the solvated emitting state and C as the unrelaxed ground state. The absence of a dark excited species could be explained by a decay shorter than its formation. The solvation times as well as the lifetimes of the emitting state populations differ from those obtained from the analysis of the FU data, but their orders of magnitude are similar. This difference most certainly arises from the crudeness of the model used for the analysis, which assumes that each species is in quasi-equilibrium and follows a first order kinetics. This is of course not the case here, as population transfer occurs on similar time scales as solvent and vibrational relaxation. As these phenomena appear differently in FU and in TA, their relative contribution to a given time constant in an analysis assuming exponential dynamics may differ. As a consequence, a time constant assigned here as a population decay may also be partially due to a relaxation process with an amount that might depend on whether it has been extracted from fluorescence or TA data.

In nonpolar solvents, species A and B also show the stimulated emission band. In this case, however, the transition from A to B is not ascribed to solvent relaxation but to vibrational relaxation as discussed above.

Figure 5 shows TA spectra recorded with **2** in ACN at different time delays after 500 nm excitation. These spectra are similar to those recorded with **1**, the main difference being the vibrational structure of the bleach and the more intense stimulated emission band. These spectra could also be analyzed with the three consecutive steps, the SADS being shown in

dx.doi.org/10.1021/jp409646g | J. Phys. Chem. A 2013, 117, 13112–13126

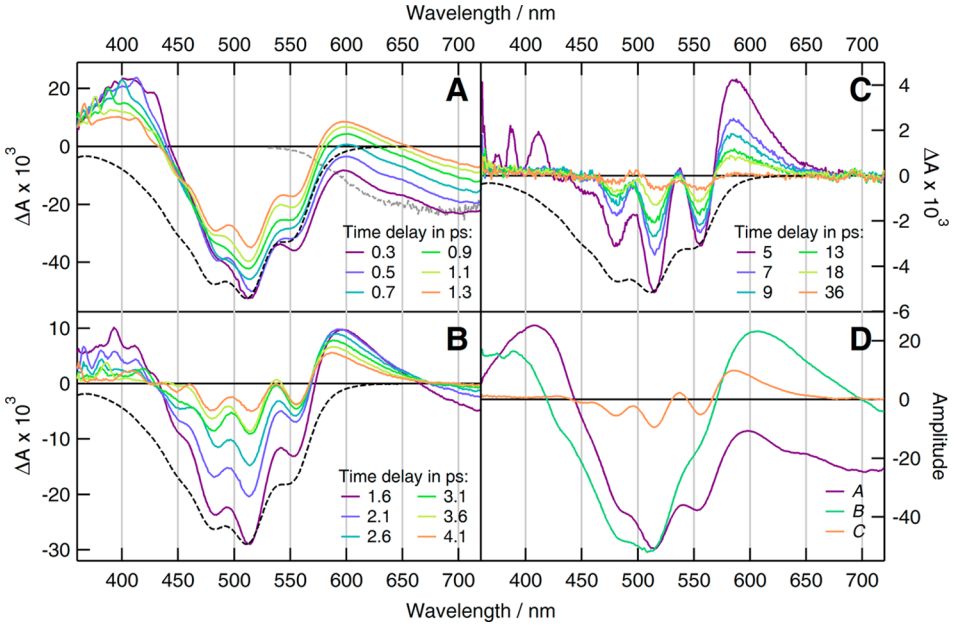

Figure 5. (A–C) Visible TA spectra measured with **2** in ACN and (D) species-associated difference absorption spectra obtained from target analysis. The dashed black line and the dashed gray line represent the scaled stationary absorption and stimulated emission spectra, respectively.

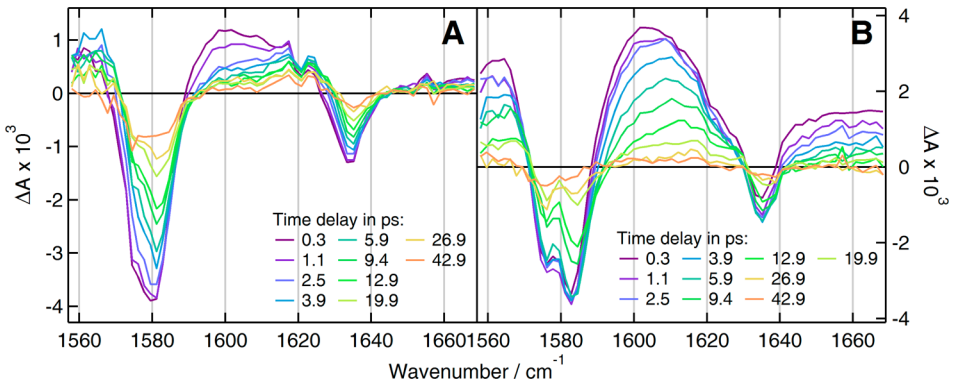

Figure 6. IR TA spectra measured with **1** in (A) ACN and (B) PeOH.

Figure 5D and the time constants listed in Table 3. These spectra can be interpreted as those of **1** in ACN, namely the first observed species is the emitting state that evolves to a dark excited state, which itself undergoes nonradiative deactivation to the unrelaxed ground state that finally equilibrates.

Like with **1**, the dark excited state cannot be seen in the long alcohols and in DD and the earliest species is the unrelaxed emitting state. In CHX, an additional step had to be included, as both unrelaxed emitting state and dark excited state can be observed.

Infrared Transient Absorption. Transient IR spectra in the C═C stretch region have been recorded with **1** in ACN, PeOH and DeOH, those in ACN and PeOH being shown in Figure 6. No measurement could be performed in the nonpolar solvents, because of the limited solubility of **1**. In all three solvents, the IR TA spectra exhibit two negative bands due to the bleach of the ground-state population. The most intense one is around 1580 cm^{-1} and is ascribed, on the basis of DFT calculations, to the interring C–C stretch, whereas the other one is at 1635 cm^{-1} and assigned to the aromatic C═C stretch. Considering the zwitterionic character of the ground state of **1** in sufficiently polar solvents, the high intensity of the 1580 cm^{-1} band is in agreement with the large variation of permanent electric dipole moment associated with the interring stretch.

Between these negative bands, broad positive features that are more intense in PeOH than in ACN are also present. Beside the decay of all bands within a few tens of picoseconds, the most prominent dynamic feature is the continuous ∼15 cm^{-1} frequency upshift of the positive band located around 1610 cm^{-1}. Target analysis of the IR TA spectra was performed using a series of consecutive first-order steps as well. In PeOH and DeOH, a good fit was obtained using three steps with the same time constants as those obtained from the visible TA measurements. The spectra associated with A and B (Figure S6) exhibit the bleach and the positive features, the most visible difference being that the main positive band shifts from 1602 to 1610 cm^{-1} by going from A to B. This small difference points to minor structural changes, in agreement with our assignment of this process to solvent relaxation. Whereas the negative bands decrease in intensities by a factor of ∼2 when going from B to C, the positive bands exhibit a stronger decrease, especially that above 1640 cm^{-1}, which almost totally vanishes. Moreover, the two other positive bands shift substantially toward the negative bands. This spectrum is typical of a hot ground state. In this case, the high frequency mode that is monitored is in the

dx.doi.org/10.1021/jp409646g | J. Phys. Chem. A 2013, 117, 13112–13126

ground state but anharmonically couples with excited low frequency modes.[37,38]

Analysis of the IR TA spectra in ACN points to the presence of a slow component that is absent in the visible TA spectra. Target analysis was performed using either (i) the three-steps model and fixing the first two time constant to 1.3 and 3 ps, or (ii) using a four steps model fixing the first three time constants to the values found by visible TA. Good fit to the data was obtained in both cases with a time constant associated with the slow component of 36 and 41 ps for i and ii, respectively. In both cases, the spectrum of species A exhibits the main positive features with a maximum at 1600 cm^{-1} which is assigned to the emitting state. In the spectrum of B, this band is weaker and peaks at 1615 cm^{-1}. Finally the spectra of C (model i) and C and D (model ii) are all very similar and resemble those assigned above to the unrelaxed, hot ground state.

Assignment of the positive TA bands to a specific vibrational mode of **1** is difficult. Nevertheless, the very large width of these positive features suggests an inhomogeneous broadening possibly due to a distribution of geometries in the excited state. This, together with the temporal frequency upshift, indicates that the excited-state dynamics of this molecule is associated with substantial structural changes. This is in full agreement with the viscosity dependence of the fluorescence lifetime that points to the involvement of modes with large amplitude motion.

Figure 7 shows IR TA spectra measured in the same spectral region with **2** in ACN, PeOH, and CHX upon 400 nm excitation. These spectra are strongly solvent dependent, contrary to what was observed with **1**. All of them are dominated by negative bands due to the depletion of the ground-state population. Those observed in ACN are tentatively ascribed to the interring C−C stretch (1570 cm^{-1}) and to aromatic C═C stretches (1602 and 1655 cm^{-1}). The intensity of all three bands decreases continuously with time and, after about 1 ps, small positive features start to rise on their high-frequency side until about 4 ps before decaying to zero on the ∼20 ps time scale. Target analysis was performed using the time constants measured by visible TA (Table 3). Like for **1**, a fourth step, with a 21 ps time constant, had to be added to account for the slow decay component that does not appear in the visible TA, the SADS being depicted in Figure S7. The spectra associated with A and B are identical and exhibit only negative bands. This confirms our assignment of species B to an excited state. If B were a highly vibrationally hot or unrelaxed ground state, its IR spectrum would show weaker bleach bands with positive bands on their low-frequency side. Such features are precisely appearing in the spectra associated with the last two species. The bleaches are more intense and the positive bands more frequency down-shifted in the spectrum of C than in that of D, indicating that C and D both correspond to the unrelaxed ground state but at different stages of its equilibration. In CHX, the two bands at low frequency are substantially narrower, closer to each other and have different relative intensities than in ACN (Figure 7B). This points to markedly different ground-state structures of **2** in these two solvents. Target analysis could be performed with the three steps model, but the first step observed in the visible TA could not be seen in the IR, in agreement with the absence of excited-state vibrational band in this spectral region. The spectra associated with the next two species correspond to the unrelaxed ground state as in ACN.

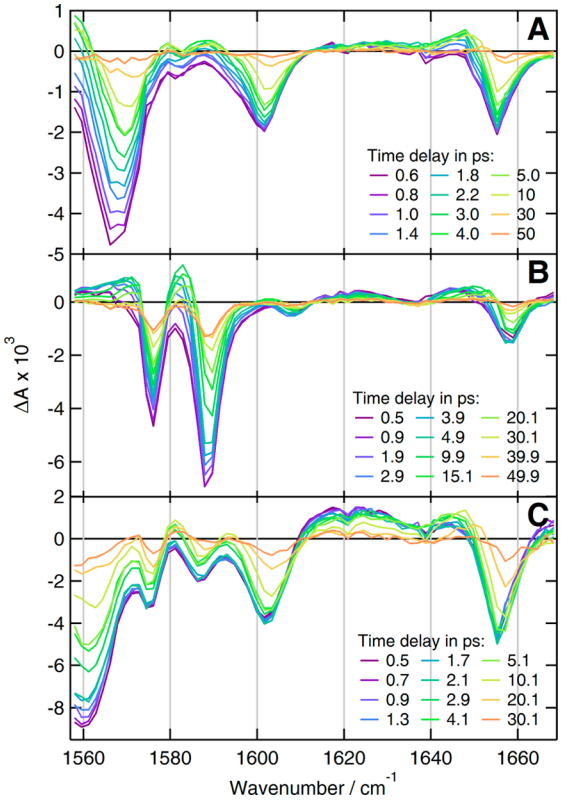

Figure 7. IR TA spectra measured with **2** in (A) ACN, (B) CHX, and (C) PeOH.

The IR TA spectra in PeOH (Figure 7C) and DeOH (not shown) look almost like the composite of those in ACN and CHX. This could indicate that two different forms of **2** that dominate in ACN and in CHX are coexisting in these medium polarity solvents. Addition of a base to a solution of **2** in PeOH (100 μL 1 M NaOH in 3 mL) did not result in significantly different IR TA spectra, indicating that the protonated form, **H-2**, does not contribute to these spectra.

The IR TA spectra measured with **2** in PeOH and DeOH show a broad positive band around 1620 cm^{-1} already at early times, contrary to those measured in ACN and CHX. Target analysis could be performed with the three steps model like in CHX. The spectrum of the first species exhibits the 1620 cm^{-1} band ascribed to the emitting state. The spectrum of the third species is typical of the unrelaxed ground state, whereas that of the second species, which decays with a 8.6 ps time constant, contains both excited- and ground-state features, indicating that two different processes might be associated with a similar time constant. Such an explanation would be compatible with two coexisting structures undergoing different nonradiative deactivation.

DISCUSSION

Qualitative Considerations. All the data presented above indicate that the excited-state dynamics of both **1** and **2** is associated with substantial structural changes, involving a mode with large amplitude motion. One evident candidate for such mode is the torsion around the interring bond. This would explain the approximately 10 times shorter fluorescence lifetime of analogue **1a**, which lacks the phenyl substituents.

According to DFT calculations, the ground-state minimum of **1** and **2** is nearly planar. An increase of the dihedral angle

dx.doi.org/10.1021/jp409646g | J. Phys. Chem. A 2013, 117, 13112−13126

between the two rings, θ, up to 90° raises the ground-state energy by more than 1.5 eV (Figure 8). The same approach for the S_1 state using TD-DFT shows that the energy of this state decreases by about the same amount upon varying θ from 0 to 90°.

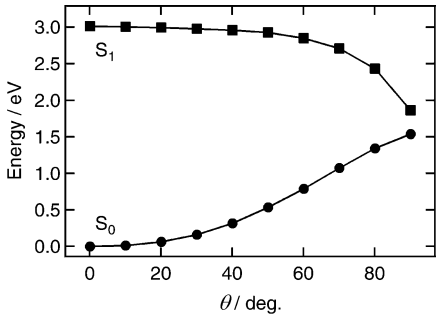

Figure 8. Calculated relative energy of **1** in the S_0 and S_1 states as a function of the interring torsion angle, θ.

Although the results of these calculations should only be considered on a qualitative basis, as the experimental transition energy is not well reproduced, they reveal a strong decrease of the S_1-S_0 gap upon increasing θ. Application of the 6-31G(d) basis set instead of the cc-pVDZ does not have a significant influence on the S_1-S_0 gap at 0°, but reduces it further at 90° for **1** and even predicts a state crossing for **2** at ∼85°. Even if these states do not cross upon twisting, distortion along additional intramolecular modes can be expected to narrow further the energy gap and to even give access to a conical intersection (COI). The α value of 0.9 obtained for **1** indicates that the excited-state decay of this molecule is essentially controlled by this torsional mode. The smaller value found for **2**, *i.e.*, α = 0.53, may seem surprising, considering the very similar volume displacement involved in the torsion around the interring bond. However, this difference might be due to a more important participation of other modes to the internal conversion and/or due to polarity effects. Both these factors may play a role: the maximum of the absorption band corresponds to higher vibronic values for **2** indicating a larger Franck−Condon displacement and the involvement of a further coordinate in addition to twisting, and the larger influence of polarity on the excited-state dynamics of **2** also signifies a more important involvement of a further mode, the solvent relaxation.

It appears from what precedes that the excited-state dynamics of **1** and **2** can be qualitatively well accounted for by the scheme illustrated in Figure 9. It is similar to that proposed to explain the ultrafast nonradiative deactivation of triphenylmethane dyes.[39] In this scheme, the transient observed in the visible TA spectra and ascribed to a dark excited state most probably corresponds to a twisted form of the excited state 'on the way' toward a COI or to a region of reduced S_1-S_0 gap. Indeed, its TA spectrum shows the same features as the emitting state except for the stimulated emission band, which is missing. Moreover, its lifetime is close to that of the emitting state.

The absence of emission can be accounted for by a small transition dipole moment due the twist angle between the two rings. This 'state' was not evidenced in the highly viscous long alcohols and the nonpolar solvents when using the three-step model. Most probably, addition of a fourth step to the analysis

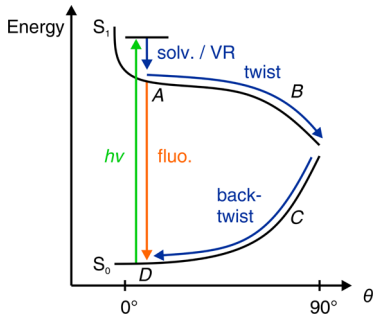

Figure 9. Schematic energy diagram accounting for the excited-state dynamics observed with **1** and **2**.

would allow its observation. However, as the three-step model resulted in a very good fit to the data, we preferred not to add any unnecessary step. According to the scheme shown in Figure 9, a twisted ground-state structure is reached after internal conversion. Relaxation to the planar equilibrium geometry involves a back-twist and should thus depend on solvent viscosity as well. Table 3 shows that the lifetime of species C obtained from the three-step analysis of the visible TA data of **1** indeed increases with solvent viscosity. A log−log plot of this time constant vs. viscosity reveals a quasi-linear dependence, as expected from eq 1 with a α value of 0.84 ± 0.08 (Figure S8). This is close to the value of 0.90 found for the lifetime of the excited state, indicating that similar large amplitude motion is involved in both processes. From Tables 2 and 3, it appears that this process is slower by a factor of ∼2 in the ground-state than the excited-state twist. This difference, that has also been observed with malachite green,[39] could be accounted for by a steeper excited-state potential. The resemblance of the TA spectrum of the twisted ground state with that of a vibrationally hot ground state is consistent with the fact that the S_1-S_0 energy gap is narrower for the twisted than for the planar molecule. This assignment does not preclude the occurrence of vibrational cooling on the same time scale as back-twist. However, this process has not been shown to depend on solvent viscosity.[29] Vibrational cooling cannot be associated with a single time scale and depends on which vibrational mode is monitored. In visible TA, only the Franck−Condon active modes are observed, whereas all the IR active vibrations can be monitored in IR TA. This explains why the slowest component observed in the IR TA experiment is, in some cases, not observable in the visible TA. This process can be ascribed to the cooling of some vibrational modes that are still non-equilibrated after the back-twist of the molecule.

For **2**, contrary to **1**, the time constant assigned to back-twist does not only depend on viscosity but also on solvent polarity, as judged from the very long time constants for CHX and DD (Figure S8). If only the polar solvents are considered, an α value of 0.33 ± 0.04 is obtained. This value does not differ much from that obtained for the excited state, especially considering the limited number of solvents. In nonpolar solvents, this time constant is larger by a factor of approximately two and seems also to increase with viscosity. This solvent polarity dependence of the back-twist of **2** is stronger than that observed for its excited-state twist. Indeed, the excited-state dynamics is slower in nonpolar than in polar solvents by a factor of less than 2, whereas this difference amounts to a factor of about 4 for the ground-state dynamics.

Whereas for **1**, the ensemble of experimental data is consistent with a more zwitterionic, i.e. more aromatic, ground

dx.doi.org/10.1021/jp409646g | J. Phys. Chem. A 2013, 117, 13112−13126

Scheme 2. Main Resonance Structures of Two Classes of Donor–Acceptor Merocyanines, Z Denoting the Zwitterionic and N the Non-Charge-Separated Character of the Corresponding Electronic Distribution, and hp and dd Standing for the Hole–Pair and Dot–Dot States in the Biradicaloid Model (See Text)[a]

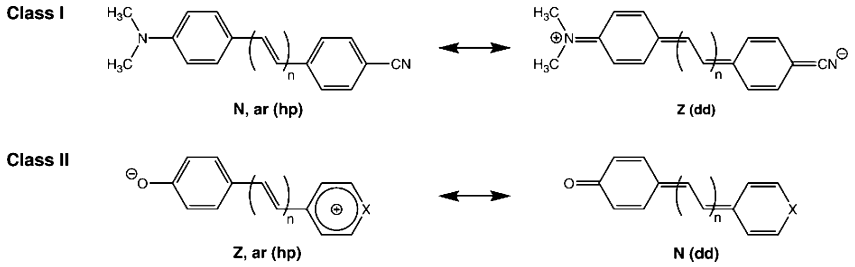

[a]Class I is characterized by the aromatic (ar) **N** and class II by the aromatic **Z** form.

state, the data obtained for **2** are more consistent with a ground-state structure of less polar, more quinoid, nature in nonpolar solvent which gains an increasingly zwitterionic character as solvent polarity rises. In an electron donor–acceptor picture, this difference in behavior can be accounted for by the stronger electron acceptor character of the pyrylium group compared to the pyridinium group. Because of this, optical excitation to the S_1 state results in an opposite change of dipole moment for **1** and **2** (negative vs positive solvatochromism). However, despite this marked difference, the excited-state dynamics of both molecules are not largely different, which is probably due to their close structural similarity. At the same time, some quantitative distinctions may be due to the difference in their excited-state electron density distributions.

Application of the Cyanine Limit Model and the Spectroscopic Hyperbola. Some features revealed in the optical properties of compounds **1** and **2** can be rationalized using the *cyanine limit (CL) model*,[27] in terms of the so-called spectroscopic hyperbola.[40,41] Both experimentally and computationally derived $S_1 \leftarrow S_0$ transition energies, $\bar{\nu}_{00}$, of merocyanines, if plotted versus the donor–acceptor strength of their end substituents, S_{DA}, represent a quasi-hyperbolic curve, with the position of a given merocyanine on the S_{DA} axis specified by the difference between the HOMO energy of the donor moiety, D, and the LUMO energy of the acceptor moiety, A.[42,43] The vertical offset of the hyperbola bottom from the abscissa is related to the mesomeric interaction between the D and A units of the compounds,[40,41] and therefore depends on the twist angle of the ground-state equilibrium. This dependence can be substantiated analytically in the framework of the valence bond model,[44] assuming that the ground- and excited-state wave functions of the D–A molecules, $\psi_{DA}(S_0)$ and $\psi_{DA}(S_1)$ can be described by the linear combination of the wave functions of two main resonance structures, zwitterionic (**Z**) and non-charge-separated (**N**), ψ_Z and ψ_N, with the mixing coefficient c:

$$\psi_{DA}(S_0) = c\psi_Z + (1 - c^2)^{1/2}\psi_N \quad (2a)$$

$$\psi_{DA}(S_1) = (1 - c^2)^{1/2}\psi_Z - c\psi_N \quad (2b)$$

For larger systems, where the aromatic character plays a role, further resonance structures become significant but are not relevant for the CL model and the spectroscopic hyperbola, if their relative contributions are the same in both states. In this case, the CL is still defined by equal **N** and **Z** contributions, and equal dipole moments in both states. Depending on which of the **N** or **Z** form is aromatic, the merocyanines belong to class I or II, respectively, as exemplified in Scheme 2.

As shown previously,[40,41] eqs 2a and 2b specify the hyperbolic dependence of the $S_1–S_0$ energy difference, $\bar{\nu}_{00}$, on S_{DA} (Figure 10). It follows from the **Z**–**N** interrelations that

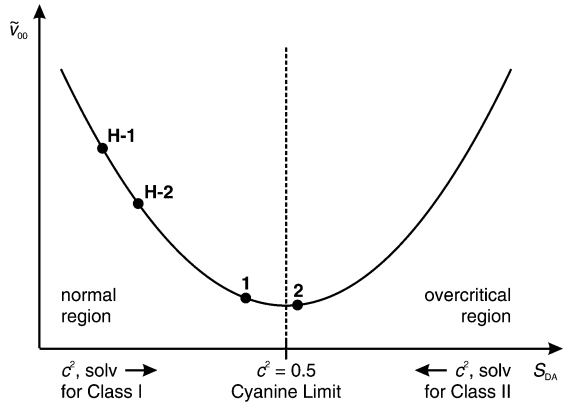

Figure 10. $S_1 \leftarrow S_0$ transition energy, $\bar{\nu}_{00}$, vs the donor–acceptor strength of the end substituents, S_{DA}, for classes I and II merocyanines and estimated locations of compounds **1** and **2** and of their protonated derivatives **H-1** and **H-2** on the hyperbolic curve.

class I and II compounds should exhibit some mirror-like π-electronic properties. In the *normal* region (Figure 10), the main ground-state valence bond wave function is of aromatic character for both classes. Therefore, class I compounds are weakly polar (more **N** character), whereas class II compounds are strongly polar (more **Z** character). The opposite holds for the excited-state wave function, hence class I compounds show positive (S_1 more polar than S_0) and class II compounds negative (S_1 less polar than S_0) solvatochromism in the *normal* region. Well-known representatives for class I compounds are the so-called twisted-intramolecular charge-transfer (TICT) compounds,[45,46] whereas the classical merocyanines or betaines, including compounds **1** and **2**, belong to class II. Although negative solvatochromic behavior is observed for the majority of class II dyes (*normal* region), some compounds with very strong D–A character exhibit a solvatochromic inversion, with positive solvatochromism over a variable fraction of the solvent polarity scale.[47] For these compounds, which belong to the *overcritical* region of the hyperbola, the ground state is less polar than the excited state. Therefore, the polarity of the ground state and, accordingly, the c^2 value increase with S_{DA} for class I compounds and decrease for class II compounds (Figure 10).

dx.doi.org/10.1021/jp409646g | J. Phys. Chem. A 2013, 117, 13112–13126

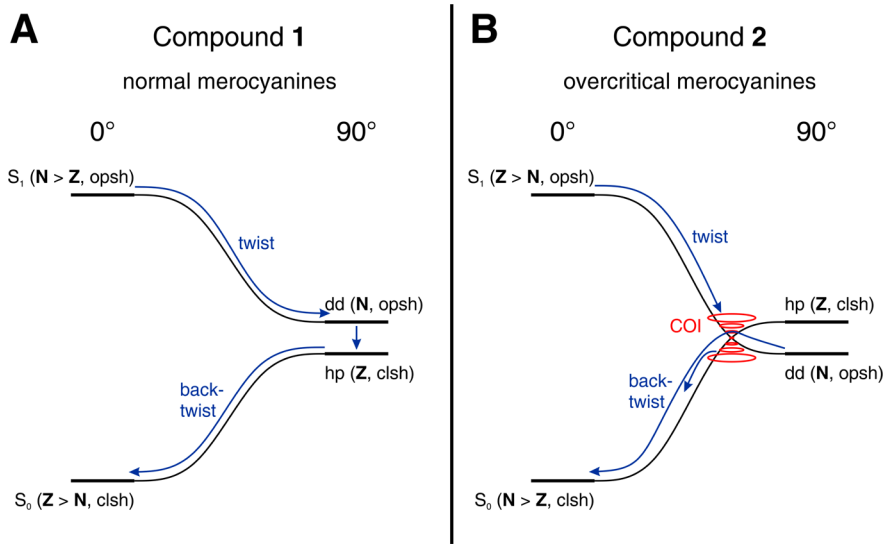

Figure 11. Electronic nature and relaxation paths for class II merocyanines **1** and **2** in the (A) *normal* and in the (B) *overcritical* region. For details, see text.

Because of the polarizing effect of the solvent, increasing solvent polarity has a similar effect as rising S_{DA} for class I compounds and an opposite effect for class II compounds as indicated by the horizontal arrows in Figure 10, the changes being in both cases in the direction of increasing the **Z** character of the ground state. For both classes, the CL point characterized by $c^2 = 0.5$ implies the minimum energy separation of the ground and excited state. The CL is therefore characterized by the most red-shifted absorption/emission and the absence of solvatochromism because the ground and excited states are equally polar.

The steady-state absorption spectra of **1** and **2**, which belong to class II, can be readily explained within this hyperbolic model. From its weak negative solvatochromism and small 0−0 energies, **1** belongs to the *normal* region and should be located near the CL point (see Figure 10). On the other hand, as **2** has a stronger acceptor and hence a larger S_{DA}, it is located on the right side of **1**, in the *overcritical* region and closer to the CL, in agreement with the weak positive solvatochromism and lower 0−0 transition energy. The S_{DA} values of both **1** and **2** drastically decrease upon protonation, which converts their very strong phenolate donor to a much weaker phenol donor. As a result, both protonated compounds are located significantly further in the *normal* region. Their relative location remains, however, unchanged, thus giving rise to an increased excitation energy for both compounds and to a lower-energy absorption for **H-2** (Figure 10). The same difference in S_{DA} between **1** and **2** and **H-1** and **H-2** does not result in the same difference in transition energy, because the unprotonated compounds are located near the flat bottom of the hyperbola, whereas the protonated forms are on the steep left wing. These trends in the optical behavior of **1** and **2** are very similar to those of their higher vinylogues reported previously.[40]

Connection between the Spectroscopic Hyperbola and the Biradicaloid Model. The discussion based on Figure 10 is valid for near-planar dyes, *i.e.*, with large electronic interaction and strong mixing between the **N** and **Z** wave functions. The so-called biradicaloid model is more relevant for molecules which spontaneously twist in the excited state as those investigated here.[48,49] At 90°, the D and A units are decoupled, and, for a *normal* system, the ground state is a so-called hole-pair, hp, state, with the doubly occupied HOMO localized on D. The excited state is associated with the transfer of one electron from D to A and corresponds to a dot-dot, dd, state, with an odd number of electrons on both units. The interaction between the hp and dd states is zero at 90° but increases strongly as the twist angle decreases. This results in a mixing of the frontier orbitals, which become delocalized over D and A at 0°, as well as in an energetic "repulsion" between the two states, which is at the origin of the shape of the S_1 and S_0 state potentials, the first going uphill and the second downhill when moving from 90° to 0° (see Figure 8). The interaction of the dd and hp states is equivalent to the mixing of the **N** and **Z** valence-bond functions employed in the CL model. We can therefore connect the CL model to the biradicaloid model and describe the electronic changes, *e.g.*, dipole moments, as the angular relaxation takes place. In the biradicaloid picture, both class I and II compounds in the normal region have a hp ground state at any twist angle, but with predominant **N** and **Z** character for class I and II, respectively (Scheme 2, l.h.s. resonance structure). The situation is the opposite in the dd excited state. On the other hand, class II compounds in the overcritical region are characterized by a dd ground state with predominant **N** character at any twist angle and a hp excited state with predominant **Z** character (Scheme 2, r.h.s. resonance structure). Because of the strong aromatic stabilization of their hp form, class I compounds are never found in the overcritical region.

An additional distinctive difference between class I and class II compounds is the dual fluorescence of TICT compounds, which necessitates a sizable energy gap not only at 0°, but also at 90°. For class II compounds, on the other hand, the S_1 and S_0 states generally come very close at 90° (Figure 11A) such that fluorescence from the twisted conformation is not observed. In this case, sufficiently strong D and A moieties can even lead to an energy reversal of the states at 90°, *i.e.* the dd state is below the hp state (Figure 11B). Such an open-shell ground state is, of course, not stable and is therefore prone to very fast angular relaxation and development into the stable closed-shell, hp state at 0°. In such case, the system is called *overcritical*, in reference to the *critical* cases where the hp and dd states are isoenergetic

dx.doi.org/10.1021/jp409646g | J. Phys. Chem. A 2013, 117, 13112−13126

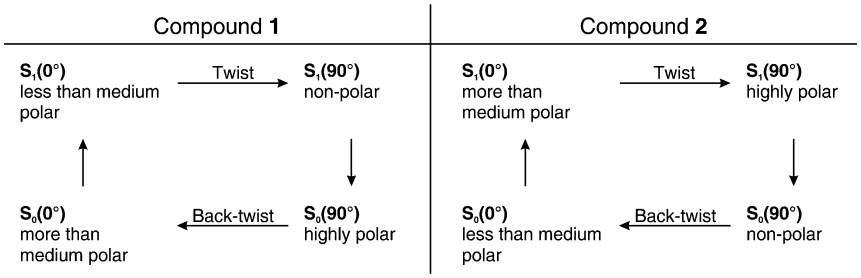

Figure 12. Dipolar properties along the relaxation paths for *normal* and *overcritical* merocyanines.

and the *normal* cases where the dd state is higher than the hp state.[48,49]

For a class II compound in the *overcritical* region, the back twist from perpendicular to planar geometry involves a real state crossing connecting the two open-shell (opsh) states at 0° and 90°, as well as the two closed-shell (clsh) ones, if only the twist as single coordinate is considered. Coupling with a further relaxation coordinate which destroys the high symmetry of the purely twisted system, *e.g.* bending or unsymmetric stretching, leads to electronic coupling and avoidance of the crossing. In a two-dimensional representation, *i.e.* the twist and one further coordinate, this corresponds to a COI (Figure 11B).[50,51] Merocyanines exhibiting this behavior can be easily recognized experimentally by their positive solvatochromic behavior.[47,52] On the other hand, *normal* merocyanines, characterized by their negative solvatochromism, show no COI on their excited-state relaxation before reaching the S_1 dd-minimum, from where ultrafast nonradiative relaxation to the hp ground-state occurs, due to their energetic proximity (Figure 11A).

It can be argued that, since *overcritical* merocyanines reach the ground-state surface at angles smaller than 90°, they do not have to relax to the dd-minimum at 90° but reverse their relaxational motion before. This is unlikely as torsional motion (or motion along any relaxation coordinate) possesses a certain inertia, and crossing a COI preferentially continues the trajectories in the forward direction (see, *e.g.*, ref 50). This has also been discussed as a reason for the high quantum yield of product formation in the visual chromophore.[48,53]

Interpretation of the Kinetic Observations. The simple hyperbolic model comprising the CL model linked to the biradicaloid model as sketched in Figure 11 helps us to understand the photophysical behavior of compounds **1** and **2**. In this case, both planar and perpendicular forms have to be considered together with their wave function and dipolar character.

The main kinetic results, illustrated in Figures S4 and S8, can be summarized as follows:

- R1: there is a significant kinetic enhancement for **2** in polar solvents in both excited- and ground-state relaxations, which is essentially absent for **1**;
- R2: compared to **1**, **2** has a reduced sensitivity to viscous friction indicative of the involvement of a further relaxation coordinate in addition to the twist;
- R3: the angular relaxation is faster for **2** than for **1** in the excited state and slower in the ground state;
- R4: the relaxation in the ground state is slower than in the excited state for both **1** and **2**.

*Polar Solvent Acceleration of the Relaxation for **2** (R1).* For merocyanines in the *normal* region, such as compound **1**, the excited-state dipole moment decreases with the angular relaxation (Figure 11A). Conversely, for **2** in the *overcritical* region, the dipole moment increases with twisting, because the excited state has more **Z** than **N** character at 0° and evolves to a very highly polar species with essentially pure **Z** character at 90° (Figure 11B). This leads to a stronger stabilization of the 90° twisted species in polar solvents and a corresponding distortion of the relaxation potential increasing the driving force for the twisting relaxation in polar solvents. As this additional driving force is absent in **1**, this model allows to understand why **2** shows an enhanced polarity dependence of its excited-state relaxation at least before crossing the COI.

In the ground-state back twisting relaxation, compound **1** evolves from a highly polar twisted species, with essentially pure **Z** character, to a less polar planar one, with more **Z** than **N** character. On the contrary, **2** starts as a nonpolar 90° twisted species and evolves to a planar species with a sizable dipole moment in agreement with a location close to CL. Therefore, the same accelerating effect of polar solvents is expected for **2** in the ground-state, and is absent for **1**. The situation is summarized in Figure 12.

*Reduced Sensitivity to Friction for **2** in Polar Solvents (R2).* Polar solvent stabilization is not directly linked to the viscosity, hence the enhanced involvement of the polar solvent relaxation as a second reaction coordinate for **2** may explain its reduced α values of around 0.5 for both S_1 and S_0 relaxations, as opposed to α values around 0.9 for compound **1**. A further factor could be the involvement of the COI for **2**, which necessitates at least one further internal relaxation coordinate in addition to the twist. This coordinate could be of high frequency, connected with smaller amplitude motions and hence less sensitivity to viscous friction.

*Acceleration of the Relaxation in the Excited State, but Slowing down in the Ground State for **2** (R3).* For *overcritical* merocyanines, the slope of the S_1 relaxation potential (Figure 11B) should be slightly larger than for *normal* merocyanines (Figure 11A), because of the correlation of planar S_1 with the twisted dd state which is lower lying for compound **2** with the stronger acceptor. This effect may be small, however, as suggested by the results in Tables 2 and 3 as well as Figure S2 for the ground-state relaxation, the lower cone of a COI has to be "circumnavigated" in the case of **2** (Figure 11B). Qualitatively speaking, low energy paths surrounding the cone of the COI necessitate a certain combination of the twisting and of a second coordinate, although the relaxation may be barrierless in both cases, without and with COI for compounds **1** and **2**. This is reflected in the statistical factor, *e.g.*, the pre-exponential factor in an Arrhenius description, which should be lower for **2** as compared to **1** and could explain its slower ground-state relaxation in the very weakly polar solvents (Figure S8).

dx.doi.org/10.1021/jp409646g | J. Phys. Chem. A 2013, 117, 13112−13126

Slower Ground-State than Excited-State Relaxation for both 1 and 2 (R4). Whereas the slower ground-state relaxation of **2** can be accounted for by the presence of a COI (Figure 11B), another factor, which could also be operative for **2**, should be invoked for **1** (Tables 2 and 3; Figures S4 and S8). According to Figure 11A, the shapes of the excited- and ground-state potentials for twist and back-twist could be identical and consequently, both processes might take place with a similar rate. However, it should be kept in mind that the model used to deduce these schemes only allows a qualitative discussion of the relaxation dynamics. Most probably, these potentials are not identical and the potential for excited-state twisting should be steeper than that for the ground-state back-twist. A definitive answer would require intensive quantum chemical calculations of both ground- and excited-state hypersurfaces, that are beyond the scope of the present investigation.

CONCLUDING REMARKS

The present study shows that for both the pyridinium and pyrylium phenolates investigated here, optical population of the Franck−Condon S_1 state is followed by torsional motion around the single bond between the two rings toward a conical intersection with the ground state or a region with a narrow gap between the excited- and ground-state potential energy surfaces. After internal conversion, the distorted molecule relaxes back to the planar ground state via a reverse twist motion. The excited-state dynamics of these donor−acceptor biaryls, though strongly dominated by structural dynamics, is also notably tuned by variations of the donor−acceptor strength of the end substituents. The close structural similarity of biaryls **1** and **2**, giving rise to qualitatively much the same structural dynamics, enables to single out the effect of donor−acceptor strength on the twisting relaxation in the excited and ground state. Other factors being equal, the following points are important: (i) the downhill slope for the twisting relaxation (as a dominating factor leading to the strong viscosity dependence); (ii) bulky substituents which can slow down the twisting relaxation; (iii) the prevailing nature of the ground- and excited-state wave functions, **Z** > **N** or **Z** < **N**; (iv) polarity changes upon excitation/de-excitation as well as upon angular twisting in both ground and excited state which can lead to additional polarity effects.

The solvatochromism is opposite for the two dyes, negative for **1** and positive for **2**. This suggests that the two compounds are found on different sides of the cyanine limit, the former in the *normal* (**Z** prevailing) and the latter in the *overcritical* region (**N** prevailing) of the spectroscopic hyperbola. As a consequence, the molecular polarity changes upon excitation/de-excitation and upon angular relaxation are also opposite and lead to enhanced polarity dependences for compound **2** for both excited- and ground-state twisting.

Overcritical merocyanines have larger donor−acceptor strength of the end substituents and, accordingly, a lower-lying twisted dd state than *normal* merocyanines. Since the planar S_1 state is correlated with the twisted dd state, *overcritical* merocyanines exhibit a steeper slope of the S_1 relaxation potential and, hence, faster excited-state twisting dynamics than *normal* merocyanines, as found for compound **2**. On the other hand, the S_0-S_1 conical intersection which is predicted for **2** slows down its ground-state relaxation kinetics as compared to **1**.

ASSOCIATED CONTENT

Supporting Information

Solvatochromic plots, fluorescence emission and excitation spectra, viscosity dependence of the fluorescence lifetime and of the back-twist time constant, stationary IR spectra, and species-associated difference IR spectra. This material is available free of charge via the Internet at http://pubs.acs.org.

AUTHOR INFORMATION

Corresponding Authors

*E-mail: (W.R.) rettig@chemie.hu-berlin.de.
*E-mail: (E.V.) eric.vauthey@unige.ch.

Notes

The authors declare no competing financial interest.

ACKNOWLEDGMENTS

The authors wish to thank the Fonds National Suisse de la Recherche Scientifique (Projects Nr. 200020-124393 and 200020_147098) as well as the University of Geneva for financial support.

REFERENCES

(1) Blanchard-Desce, M.; Alain, V.; Bedworth, P. V.; Marder, S. R.; Fort, A.; Runser, C.; Barzoukas, M.; Lebus, S.; Wortmann, R. Large Quadratic Hyperpolarizabilities with Donor−Acceptor Polyenes Exhibiting Optimum Bond Length Alternation: Correlation Between Structure and Hyperpolarizability. *Chem.—Eur. J.* **1997**, *3*, 1091−1104.

(2) Boeglin, A.; Barsella, A.; Fort, A.; Mançois, F.; Rodriguez, V.; Diemer, V.; Chaumeil, H.; Defoin, A.; Jacques, P.; Carré, C. Optical Properties and Progressive Sterical Hindering in Pyridinium Phenoxides. *Chem. Phys. Lett.* **2007**, *442*, 298−301.

(3) Kang, H.; Facchetti, A.; Zhu, P.; Jiang, H.; Yang, Y.; Cariati, E.; Righetto, S.; Ugo, R.; Zuccaccia, C.; Macchioni, A.; et al. Exceptional Molecular Hyperpolarizabilities in Twisted π-Electron System Chromophores. *Angew. Chem., Int. Ed.* **2005**, *44*, 7922−7925.

(4) Isborn, C. M.; Davidson, E. R.; Robinson, B. H. Ab Initio Diradical/Zwitterionic Polarizabilities and Hyperpolarizabilities in Twisted Double Bonds. *J. Phys. Chem. A* **2006**, *110*, 7189−7196.

(5) Kang, H.; Facchetti, A.; Jiang, H.; Cariati, E.; Righetto, S.; Ugo, R.; Zuccaccia, C.; Macchioni, A.; Stern, C. L.; Liu, Z.; et al. Ultralarge Hyperpolarizability Twisted π-Electron System Electro-Optic Chromophores: Synthesis, Solid-State and Solution-Phase Structural Characteristics, Electronic Structures, Linear and Nonlinear Optical Properties, and Computational Studies. *J. Am. Chem. Soc.* **2007**, *129*, 3267−3286.

(6) Liu, L.; Xue, Y.; Wang, X.; Chu, X.; Yang, M. Theoretical Study of Static (Hyper)polarizabilities of Twisted Intramolecular Charge Transfer Chromophores. *Int. J. Quantum Chem.* **2011**, *112*, 1086−1096.

(7) Reichardt, C. Solvatochromic Dyes as Solvent Polarity Indicators. *Chem. Rev.* **1994**, *94*, 2319−2358.

(8) Barbara, P. F.; Walker, G. C.; Smith, T. P. Vibrational Modes and the Dynamic Solvent Effect in Electron and Proton Transfer. *Science* **1992**, *256*, 975−981.

(9) Johnson, A. E.; Levinger, N. E.; Jarzeba, W.; Schlief, R. E.; Kliner, D. A. V.; Barbara, P. F. Experimental and Theoretical Study of Inhomogeneous Electron Transfer in Betaine: Comparison of Measured and Predicted Spectral Dynamics. *Chem. Phys.* **1993**, *176*, 555−574.

(10) Reid, P. J.; Barbara, P. F. Dynamic Solvent Effect on Betaine-30 Electron Transfer Kinetics in Alcohols. *J. Phys. Chem.* **1995**, *99*, 3554−3565.

(11) Lobaugh, J.; Rossky, P. J. Computer Simulation of the Excited State Dynamics of Betaine-30 in Acetonitrile. *J. Phys. Chem. A* **1999**, *103*, 9432−9447.

(12) Kovalenko, S. A.; Eilers-König, N.; Senyushkina, T.; Ernsting, N. P. Charge Transfer and Solvation of Betaine-30 in Polar Solvents: A Femtosecond Broadband Transient Absorption Study. *J. Phys. Chem. A* **2001**, *105*, 4834−4843.
(13) Zhao, X.; Burt, J. A.; McHale, J. L. Resonance Raman Analysis of Nonlinear Solvent Dynamics: Betaine-30 in Ethanol. *J. Chem. Phys.* **2004**, *121*, 11195−11201.
(14) Ishida, T.; Rossky, P. J. Consequences of Strong Coupling between Solvation and Electronic Structure in the Excited State of a Betaine Dye. *J. Phys. Chem. B* **2008**, *112*, 11353−11360.
(15) Kharlanov, V.; Rettig, W. Experimental and Theoretical Study of Excited-State Structure and Relaxation Processes of Betaine-30 and of Pyridinium Model Compounds. *J. Phys. Chem. A* **2009**, *113*, 10693−10703.
(16) Duvanel, G.; Grilj, J.; Chaumeil, H.; Jacques, P.; Vauthey, E. Ultrafast Excited-State Dynamics of a Series of Zwitterionic Pyridinium Phenoxides with Increasing Sterical Hindering. *Photochem. Photobiol. Sci.* **2010**, *9*, 908−915.
(17) Malval, J.-P.; Chaumeil, H.; Rettig, W.; Kharlanov, V.; Diemer, V.; Ay, E.; Morlet-Savary, F.; Poizat, O. Excited-State Dynamics of Phenol-Pyridinium Biaryl. *Phys. Chem. Chem. Phys.* **2012**, *14*, 562−574.
(18) Nekhoroshev, M. V.; Okhlobystin, O. Y. Sterically Hindered Phenols in a Series of Pyrylium Salts. Oxidative Dehydrogenation of Pyrans. *Zh. Org. Khim. (Russ. J. Org. Chem.)* **1977**, *13*, 1294−1300.
(19) Morandeira, A.; Engeli, L.; Vauthey, E. Ultrafast Charge Recombination of Photogenerated Ion Pairs to an Electronic Excited State. *J. Phys. Chem. A* **2002**, *106*, 4833−4837.
(20) Duvanel, G.; Banerji, N.; Vauthey, E. Excited-State Dynamics of Donor-Acceptor Bridged Systems Containing a Boron-Dipyrromethene Chromophore: Interplay between Charge Separation and Reorientational Motion. *J. Phys. Chem. A* **2007**, *111*, 5361−5369.
(21) Banerji, N.; Duvanel, G.; Perez-Velasco, A.; Maity, S.; Sakai, N.; Matile, S.; Vauthey, E. Excited-State Dynamics of Hybrid Multichromophoric Systems: Toward an Excitation Wavelength Control of the Charge Separation Pathways. *J. Phys. Chem. A* **2009**, *113*, 8202−8212.
(22) Bredenbeck, J.; Hamm, P. Versatile Small Volume Closed-Cycle Flow Cell System for Transient Spectroscopy at High Repetition Rates. *Rev. Sci. Instrum.* **2003**, *74*, 3188−3189.
(23) Frisch, M. J.; Trucks, G. W.; Schlegel, H. B.; Scuseria, G. E.; Robb, M. A.; Cheeseman, J. R.; Scalmani, G.; Barone, V.; Mennucci, B.; Petersson, G. A.; et al. *Gaussian 09 (revision A1)*, Gaussian: Wallingford, CT, 2009.
(24) Suppan, P.; Ghoneim, N. *Solvatochromism*; The Royal Society of Chemistry: Cambridge, U.K., 1997.
(25) Jacques, P.; Graff, B.; Diemer, V.; Ay, E.; Chaumeil, H.; Carré, C.; Malval, J.-P. Negative Solvatochromism of a Series of Pyridinium Phenolate Betaine Dyes with Increasing Steric Hindrance. *Chem. Phys. Lett.* **2012**, *531*, 242−246.
(26) Lide, D. R., *Handbook of Chemistry and Physics*, 90th ed.; CRC Press: Boca Raton, FL, 1009.
(27) Bourhill, G.; Bredas, J.-L.; Cheng, L.-T.; Marder, S. R.; Meyers, F.; Perry, J. W.; Tiemann, B. G. Experimental Demonstration of the Dependence of the First Hyperpolarizability of Donor-Acceptor-Substituted Polyenes on the Ground-State Polarization and Bond Length Alternation. *J. Am. Chem. Soc.* **1994**, *116*, 2619−2620.
(28) Horng, M. L.; Gardecki, J. A.; Papazyan, A.; Maroncelli, M. Subpicosecond Measurements of Polar Solvation Dynamics: Coumarin 153 Revisited. *J. Phys. Chem.* **1995**, *99*, 17311−17337.
(29) Pigliucci, A.; Duvanel, G.; Daku, L. M. L.; Vauthey, E. Investigation of the Influence of Solute-solvent Interactions on the Vibrational Energy Relaxation Dynamics of Large Molecules in Liquids. *J. Phys. Chem. A* **2007**, *111*, 6135−6145.
(30) Velsko, S. P.; Fleming, G. R. Solvent Influence on Photochemical Isomerisations: Photophysics of DODCI. *Chem. Phys.* **1982**, *65*, 59−70.
(31) Kramers, H. A. Brownian Motion in a Field of Force and the Diffusion Model of Chemical Reactions. *Physica* **1940**, *7*, 284−304.
(32) Hicks, J.; Vandersall, M.; Babarogic, Z.; Eisenthal, K. B. The Dynamics of Barrier Crossings in Solution: The Effect of a Solvent Polarity-Dependent Barrier. *Chem. Phys. Lett.* **1985**, *116*, 18−24.
(33) van Stokkum, I. H. M.; Larsen, D. S.; van Grondelle, R. Global and Target Analysis of Time-Resolved Spectra. *Biochim. Biophys. Acta, Bioenerg.* **2004**, *1657*, 82−104.
(34) Perez-Lustres, J. L.; Rodriguez-Prieto, F.; Mosquera, M.; Senyushkina, T. A.; Ernsting, N. P.; Kovalenko, S. A. Ultrafast Proton Transfer to Solvent: Molecularity and Intermediates from Solvation- and Diffusion-Controlled Regimes. *J. Am. Chem. Soc.* **2007**, *129*, 5408−5418.
(35) Grilj, J.; Zonca, C.; Daku, L. M. L.; Vauthey, E. Photophysics of the Galvinoxyl Free Radical Revisited. *Phys. Chem. Chem. Phys.* **2012**, *14*, 6345−6351.
(36) Grilj, J.; Buchgraber, P.; Vauthey, E. Excited-State Dynamics of Wurster's Salts. *J. Phys. Chem. A* **2012**, *116*, 7516−7522.
(37) Hamm, P.; Ohline, S. M.; Zinth, W. Vibrational Cooling after Ultrafast Photoisomerisation of Azobenzene Measured by fs Infrared Spectroscopy. *J. Chem. Phys.* **1997**, *106*, 519−529.
(38) Koch, M.; Rosspeintner, A.; Adamczyk, K.; Lang, B.; Dreyer, J.; Nibbering, E. T. J.; Vauthey, E. Real-Time Observation of the Formation of Excited Radical Ions in Bimolecular Photoinduced Charge Separation: Absence of the Marcus Inverted Region Explained. *J. Am. Chem. Soc.* **2013**, *135*, 9843−9848.
(39) Fita, P.; Punzi, A.; Vauthey, E. Local Viscosity of Binary Water + Glycerol Mixtures at Liquid/Liquid Interfaces Probed by Time-Resolved Surface Second Harmonic Generation. *J. Phys. Chem. C* **2009**, *113*, 20705−20712.
(40) Rettig, W.; Dekhtyar, M. L.; Tolmachev, A. I.; Kurdyukov, V. V. Two Heterocyclic Merocyanine Classes and their Optical Properties in Relation to the Donor-Acceptor Strength of End Substituents. *Chem. Heterocycl. Compd.* **2012**, *47*, 1244−1257.
(41) Lasogga, L.; Rettig, W.; Otto, H.; Wallat, I.; Bricks, J. Model Systems for the Investigation of the Opsin Shift in Bacteriorhodopsin. *J. Phys. Chem. A* **2010**, *114*, 2179−2188.
(42) Dekhtyar, M.; Rettig, W. Polyenic/Polymethinic Relationships for Donor-Acceptor Substituted Stilbenoids: Structural, Electronic and Spectroscopic Aspects. *Phys. Chem. Chem. Phys.* **2001**, *3*, 1602−1610.
(43) Rettig, W.; Dekhtyar, M. Merocyanines: polyene−polymethine transition in donor-acceptor-substituted stilbenes and polyenes. *Chem. Phys.* **2003**, *293*, 75−90.
(44) Platt, J. R. Wavelength Formulas and Configuration Interaction in Brooker Dyes and Chain Molecules. *J. Chem. Phys.* **1956**, *25*, 80−105.
(45) Grabowski, Z. R.; Rotkiewicz, K.; Rettig, W. Structural Changes Accompanying Intramolecular Electron Transfer: Focus on Twisted Intramolecular Charge-Transfer States and Structures. *Chem. Rev.* **2003**, *103*, 3899−4031.
(46) Rettig, W. Charge Separation in Excited States of Decoupled Systems—TICT Compounds and Implications Regarding the Development of New Laser Dyes and the Primary Process of Vision and Photosynthesis. *Angew. Chem., Int. Ed.* **1986**, *25*, 971−988.
(47) Domínguez, M.; Rezende, M. C. Towards a Unified View of the Solvatochromism of Phenolate Betaine Dyes. *J. Phys. Org. Chem.* **2010**, *23*, 156−170.
(48) Bonačić-Koutecký, V.; Koutecký, J.; Michl, J. Neutral and Charged Biradicals, Zwitterions, Funnels in S1, and Proton Translocation: Their Role in Photochemistry, Photophysics, and Vision. *Angew. Chem., Int. Ed.* **1987**, *26*, 170−189.
(49) Michl, J.; Bonačić-Koutecký, V., *Electronic Aspects of Organic Photochemistry*. Wiley: New York, 1990.
(50) Sanchez-Galvez, A.; Hunt, P.; Robb, M. A.; Olivucci, M.; Vreven, T.; Schlegel, H. B. Ultrafast Radiationless Deactivation of Organic Dyes: Evidence for a Two-State Two-Mode Pathway in Polymethine Cyanines. *J. Am. Chem. Soc.* **2000**, *122*, 2911−2924.
(51) Bernardi, F.; Olivucci, M.; Robb, M. A. Potential Energy Surface Crossings in Organic Photochemistry. *Chem. Soc. Rev.* **1996**, *25*, 321−328.

(52) Kulinich, A. V.; Ishchenko, A. A. Merocyanine Dyes: Synthesis, Structure, Properties, Application. *Russ. Chem. Rev.* **2009**, *78*, 141−164.
(53) Honig, B.; Warshel, A.; Karplus, M. Theoretical Studies of the Visual Chromophore. *Acc. Chem. Res.* **1975**, *8*, 92−100.